Beyond surface nanoindentation: Combining static and dynamic nanoindentation to assess intrinsic mechanical properties of chemical vapor deposition amorphous silicon oxide (SiOx) and silicon oxycarbide (SiOxCy) thin films

Maxime Puyo, Konstantina Christina Topka, Babacar Diallo, Raphaël Laloo, Cécile Genevois, Pierre Florian, Thierry Sauvage, Diane Samelor, François Senocq, Hugues Vergnes, et al.

Article

Beyond surface nanoindentation: combining static and dynamic nanoindentation to assess intrinsic mechanical properties of Chemical Vapor Deposition amorphous silicon oxide (SiO_x) and silicon oxycarbide (SiO_xC_y) thin films.

Maxime Puyo [a], Konstantina Christina Topka [a,b], Babacar Diallo [c], Raphaël Laloo [a], Cécile Genevois [c], Pierre Florian [c], Thierry Sauvage [c], Diane Samelor [a], François Senocq [a], Hugues Vergnes [b], Brigitte Caussat [b], Marie-Joëlle Menu [a], Nadia Pellerin [c], Constantin Vahlas [a], Viviane Turq [a]

[a] Inter-university materials research and engineering center (CIRIMAT), Université de Toulouse, CNRS, Université Toulouse 3 - Paul Sabatier, 118 Route de Narbonne, 31062 Toulouse cedex 9 - France

[b] Chemical engineering laboratory (LGC), Université de Toulouse INPT, CNRS, 4 Allée Emile Monso, Toulouse, 31030, France

[c] Extreme conditions and materials: high temperature and irradiation (CEMHTI), Université d'Orléans, UPR3079 CNRS, 1D avenue de la Recherche Scientifique, 45071, Orléans, Cedex 2, France

Corresponding author: Ass. Pr. Viviane Turq, turq@chimie.ups-tlse.fr, Tel: (33) 5 61 55 62 84, CIRIMAT, 118 Route de Narbonne, 31062 Toulouse cedex 9 - France

Abstract

Nanoindentation is a well-known technique to assess the mechanical properties of bulk materials and films. Despite that, nanoindentation of thin films is not straightforward, given that the measured properties are composite information from a film/substrate system and

depend on the indentation depth. By using dynamic indentation experiments and analytical or empirical models, we assessed the intrinsic film properties of chemical vapor deposited silicon oxide (SiO_x) and silicon oxycarbide (SiO_xC_y) thin films with thicknesses ranging from 60 to 700 nm. In this work, the Bec rheological model and several mixing laws were reviewed. Measured Young modulus appeared to be affected by the substrate properties more than hardness: for the thinnest films, moduli were measured at *ca.* 90 GPa whereas intrinsic moduli were calculated at *ca.* 50 GPa. Using calculated intrinsic film modulus and hardness, it was possible to establish correlations between these properties, the chemical composition and the structural organization of the films.

Keywords: chemical vapor deposition coatings, nanoindentation, models, intrinsic film properties, silicon oxide, silicon oxycarbide, thin films.

1. Introduction

The recent development of (multi-)functional nanometric films was made possible by the evolution of thin film deposition technologies and the flourishing of advanced characterization techniques [1]. Silicon-oxide-based coatings such as silicon oxides (SiO_x [2,3]), silicon oxycarbides (SiO_xC_y [4]) or silicon oxynitrides (SiO_xN_y [5]) have been studied in detail and several deposition approaches have been published for high quality dense films, including wet chemistry-based methods [6] or gas-phase-deposition-based [4,5,7]. The resulting films have proven themselves attractive as multifunctional materials, like anti-corrosion, anti-reflective or diffusion barrier coatings. Such films can be applied for the encapsulation of systems for protection against humidity [8], oxygen, ambient contaminants and mechanical damages [9]. These barrier properties can be correlated with the characteristics of the films (thickness [8],

chemical composition [10], network density [11], inter alia), which in turn, can be tuned by modifying their deposition conditions [10,12].

Nanoindentation characterization and the pioneering work of Oliver and Pharr [13] allowed probing shallow indentation depths and conveniently assessing the Young modulus (E) and Hardness (H) of heterogeneous materials and films. Still, coated systems characterization by nanoindentation is not straightforward: substrate properties affect the measured values of E and H when the elastic and plastic deformations (respectively) are no longer confined within the film. This substrate contribution is all the more likely to be probed as films become very thin.

A first solution to avoid the substrate contribution is to work at shallow indentation depth and low normal loads, taking advantage of the precision of nanoindentation. Classically, the substrate contribution is considered negligible when the relative indentation depth (h/t, i.e. the indentation depth h divided by the thickness t of the film) is below 0.1, based on Bückle's work [14]. Under this assumption, measured E and H are considered equal to the intrinsic film modulus and hardness (quoted, respectively, E_f and H_f). This rule has been widely adopted in nanoindentation studies as it gives satisfying results for systems where the film and the substrate present relatively similar mechanical properties. However, Bückle 10 % rule can be too loose or too strict, depending on several factors affecting the elastic and plastic deformation of the film and the substrate. Among other factors, the ratios H_f/E_f and E_f/E_s are to consider carefully as a low H_f/E_f value or a substrate significantly stiffer than the film may make the substrate contribution sensible for $h/t < 0.1$ [15–17]. The critical value of h/t below which E_f and H_f can no longer be assessed by means of straightforward indentation is complex to predict as it depends on numerous interacting factors sometimes not easily accessible for thin films.

As a consequence, another approach has been developed to access intrinsic properties of films; this method is based on mathematical modeling of the composite mechanical properties of the

film/substrate system. Several models have been proposed to remove, or at least reduce, the substrate contribution from the measured mechanical properties and thus access the intrinsic film properties [18]. These approaches are still underused compared to the Bückle's 10 % rule, as they are comparatively more complex and require mechanical characterization of the film and/or of the substrate at several indentation depths. Still, determining the intrinsic film properties is of interest and these model-based methods may be applied in situations where the Bückle's rule cannot be reasonably used (e.g. for a few nanometer-thin films, multilayer systems or when investigating superficial phenomena …).

Within this context, in order to assess the intrinsic mechanical properties of amorphous silicon oxide and silicon oxycarbide thin films processed on silicon Si(100) substrates by thermal Chemical Vapor Deposition (CVD), the present work deals with the evaluation of the main published models for the determination of E_f and H_f. We compare the obtained values to E and H measured by classical static indentation at shallow indentation depths and discuss these properties with regard to the deposition temperature (T_d) of the films, their chemical composition and structure.

2. Materials and Methods

2.1. Silicon oxide and oxycarbide films

Two sets of films deposited on 280 µm thick Si(100) substrates (provided by Neyco) are investigated: "TEOS" films deposited from tetraethyl orthosilicate ($SiC_8H_{20}O_4$, TEOS) and "HMDS" films deposited from a dual-precursor chemistry involving TEOS and hexamethyldisilazane ($Si_2NC_6H_{19}$, HMDS). For both, deposition was performed at deposition temperatures (T_d) ranging from 360°C to 550°C; details can be found in two previous articles [10,12]. For each set, two subsets are defined, namely as thin and thick films with t of

about 100 nm and superior to 400 nm, respectively, obtained by adjusting the deposition time under the same process conditions (as summarized in Table 1).

Both TEOS and HMDS films are amorphous according to X-ray and electron diffraction characterizations and the structure and chemical composition of both have been characterized by Fourier transform infrared spectrometry and Ion Beam Analysis (not shown). Roughness has been measured using atomic-force microscopy (AFM) (size of image: 1 µm²) and t has been measured by spectroscopic ellipsometry. All films present a low roughness with a root mean square roughness parameter lying in the range 0.5 to 5 nm.

TEOS films are partially hydrated silicon oxides (SiO_x), with their network hydration decreasing as T_d increases from 400 to 550°C, and subsequently their hydrogen content decreasing from 8 to 5 at.%) [12]. HMDS films have tunable chemical composition depending on T_d: they consist of silicon oxycarbides (SiO_xC_y) containing CH_3 moieties (with hydrogen content between 8 and 17 at.%) at low T_d (i.e. below 500°C) and they evolve to silicon oxides at higher temperature of 500 and 550°C (with constant hydrogen content of about. 7 at.%) [10]. Because of this compositional evolution, for every film set, the increase of T_d results in the increase of the network cross-linking. This network densification is beneficial to the barrier properties illustrated by the decrease of the etching rate of the films when immersed in an acidic solution following the P-etch protocol [10,12].

2.2. Mechanical characterization methods

Mechanical properties (*i.e.* Young modulus and hardness) were characterized by nanoindentation using an UltraNanoIndenter apparatus from CSM Instruments (Anton Paar) with a modified Berkovich diamond indenter. The displacement of the indenter is measured relatively to a spherical reference, located apart from the indenter, through a differential capacitive sensor, thus allowing to consider the thermal drift. Two kinds of experiments were

carried out: static to measure the apparent Young modulus and hardness (E and H, respectively) of the film/substrate systems and dynamic nanoindentation to determine the intrinsic Young modulus and hardness of the films (E_f and H_f, respectively).

During static nanoindentation experiment, a gradually increasing normal force was applied up to a maximum value of 0.5 mN. This maximal load was maintained for 30 s, after which the force was gradually decreased to 0 mN. The loading and unloading rates were set to 1 $mN.min^{-1}$. E and H were calculated from load vs. depth curves using the Oliver and Pharr method [13]. Each sample was probed with this method on a minimum of 5 different locations on the sample surface. Before each sample characterization an indentation on fused silica standard has been performed to control the tip shape and calibration. This characterization allows an important accuracy for the measurements, with a systematic error of *ca.* 3 %. Systematic error has been evaluated by static nanoindentation on fused silica standards at 30 mN, with 10 distinct locations probed. E was experimentally found equal to 71.3 ± 0.7 GPa (with a certified Young modulus of 73.3 ± 0.3 GPa). The bare Si(100) substrate was also characterized in the same way, in order to assess substrate Young modulus and hardness (E_s and H_s). These were found equal to 172 ± 4 GPa and 15.3 ± 0.4 GPa, respectively. As shown in Figure 1, only one value of h is probed at a time by static indentation.

Dynamic nanoindentation experiments were carried out by operating the apparatus in the so-called Linear Sinus Loading mode. In this mode, a gradually increasing normal force with oscillations was applied until a maximum load (between 10 and 30 mN depending on t). This load was maintained for 30 s, then gradually decreased to 0 mN without oscillations. The loading rate was set at 3 $mN.min^{-1}$, oscillation amplitude and frequency were set respectively at 0.5 mN and 12 Hz, and the unloading rate was set at 30 $mN.min^{-1}$. Each sample was probed at 3 different locations, at least. The oscillating load allows to access local load and unload curves at several h which were exploited with the Oliver and Pharr method, allowing to

calculate local values of Young modulus and hardness for each value of h probed, as schematized in Figure 1. From these local values, experimental curves of E (or H) vs. h/t are obtained. These curves will be used as experimental input for the determination of E_f (or H_f) with the mathematical models, as explained below.

For disambiguation purposes, dynamic indentation local values of Young modulus and hardness are noted E(h) and H(h), respectively, as opposed to static indentation E and H. In order to prevent biases due to tip defects and surface roughness, any data obtained for $h < 50$ nm were systematically discarded. This 50 nm threshold was experimentally set using fused silica standards.

As shown in Figure 1, whether assessed by static or dynamic indentation, the values of the film/substrate system Young modulus and hardness range between E_f and E_s, and H_f and H_s, respectively.

2.3. Determination of the intrinsic film mechanical properties

Several models have been proposed to remove substrate contribution during the indentation of films. Most of these models were developed and verified on controlled systems for which both films and substrates had known mechanical properties (Au/Si [19], Al/glass, Al/sapphire, Al/Si [20], Ni/Cu [21], TiO_2/Ti_6Al_4V alloy [22] etc.). Only few authors have tested models outside ideal conditions and on systems comparable to the present ones, both in terms of thickness range or chemical composition [23,24]. For this reason, we proof-checked various models from the literature in order to select the most suitable ones. By fitting the models with experimental E(h) vs. h/t (or H(h) vs. h/t) curves, E_f and H_f can be determined among other output model parameters. The fitting process of the model to the experimental curves of E(h) vs. h/t (or H(h) vs. h/t) is based on the reduction of χ^2_m by the optimization of the values

of the model output parameters. χ^2_m is defined as the mean value of χ^2, as shown by Equations 1 and 2 (respectively for the Young modulus and the hardness).

$$\chi^2{}_m = \frac{1}{N}\sum_{i=1}^{N}\chi^2(h_i) = \frac{1}{N}\sum_{i=1}^{N}\frac{\left(E_{exp}(h_i) - E_{mod}(h_i)\right)^2}{E_{mod}(h_i)} \quad (1)$$

$$\chi^2{}_m = \frac{1}{N}\sum_{i=1}^{N}\chi^2(h_i) = \frac{1}{N}\sum_{i=1}^{N}\frac{\left(H_{exp}(h_i) - H_{mod}(h_i)\right)^2}{H_{mod}(h_i)} \quad (2)$$

where h_i is the local probed indentation depth (h_1 is the minimal indentation depth allowing measurement without biases and it is superior to 50 nm, h_N is the maximal indentation depth), $E_{exp}(h_i)$ (or $H_{exp}(h_i)$), the value of E(h) (or H(h)) experimentally measured at h_i and $E_{mod}(h_i)$ (or $H_{mod}(h_i)$), the value of E(h) (or H(h)) calculated with the model selected at h_i.

The determination of the E_f and H_f implies two hypotheses. The first hypothesis is that films deposited under the same conditions present identical chemical composition and structural organization. As a consequence, thin films and thick films should present identical E_f and H_f.

The second hypothesis assumes that each sample consists of a homogeneous film with constant E_f and H_f throughout the indentation depth. This hypothesis is supported by previous studies that revealed the bulk of the TEOS and HMDS films present homogeneous chemical composition and structural organization without noticeable porosity nor visible cavities[10,12]. However, it neglects the presence of surface modifications formed by hydration or contamination due to atmospheric exposure [25]. Such a superficial 10 nm-thick layer containing 4 at.% of carbon has been previously observed for 120 nm-thick-TEOS-like samples [12]. Due to higher hydration and to the presence of organic moieties [25–28], this superficial layer is expected to present lower Young modulus and hardness. Nevertheless, it

could be overlooked due to its thinness compared to the values of t (from 63 to 713 nm, as shown in Table 1) and because, as previously mentioned, only the data obtained for $h \geq 50$ nm are considered.

3. Results and discussion

3.1. Static indentation results

E and H were measured by static indentation experiments for TEOS and HMDS samples. The obtained values are displayed in Table 2 and the graphical representations of these results are plotted in Figure 2 and Figure 3 for TEOS films and in Figure 4 for HMDS films.

As expected, E is systematically higher for thin than for thick films, due to the higher influence of the silicon substrate (E_s has been found equal to 172 GPa). The values of E for thin films lie between 1.4 times (for TEOS films deposited at 500°C) to 3.1 times higher (for HMDS films deposited at 500°C) than the values found for corresponding thick films. Similarly, most of the hardness values of thin films are superior to those of the thick ones. One exception is for TEOS films deposited at T_d = 400°C: the thick film presents a value of H that is significantly higher than the one found for the corresponding thin film and also higher than the values measured for the rest of the thick films. Also, as expected, H values vary less than E values between thin and thick films (with thin films hardness *ca.* 1.3 times higher to equivalent thick films hardness) due to the smaller contribution of the substrate on hardness than on Young modulus.

The presence of hydrated and organic moieties is known to generally decrease the value of E and H for silicon oxide materials. Classically, silicon oxides have E and H ranging, respectively, from 73 to 20 GPa and from 8 to 5 GPa depending on the level of hydration [25,26,28]. Silicon-oxide-based materials containing organic moieties can be found with E between 20 and 3 GPa and H between 3 and 0.2 GPa depending on the content of

organic carbon [11,27,29]. Considering these expected E_f and H_f values and the known E_s and H_s values, TEOS and HMDS films may present a H_f/E_f ratio of about 0.1-0.3 and a E_f/E_s ratio in the range of 0.4 to 0.1 and 0.1 to 0.01, respectively. Therefore, the substrate contribution can be assumed limited for the thick films as $h/t \leq 0.2$ [15–17] and it is possible to consider that E and H measured for thick films are good estimations of E_f and H_f.

As shown in Table 2, thick films present values of E and H in good agreement with the expected values of the literature discussed previously. TEOS thick films show higher values of E and H than HMDS thick films, attributed to lower hydration and the absence of CH_3 moieties (contrary to HMDS films with $T_d < 500$°C) [10,12].

TEOS values of E and H seem to increase slightly with the increase of T_d, with exception of the values found for TEOS-400°C-525nm, which presents surprisingly high values of E and H (62 ± 2 GPa and 7.2 ± 0.4 GPa, respectively). This evolution may be related to the dehydration and the increasing network cross-linking of the TEOS films with the increase of T_d as previously reported by Diallo et al. [12] and by Ponton et al. for similar films [3].

For HMDS thick films, neither E nor H show a clear evolution as a function of T_d and both seem to fluctuate around 32 and 2.4 GPa, respectively. This absence of a correlation between E (and H) and T_d was not expected, considering the increasing network cross-linking of HMDS films with the increase of T_d and the fact that the chemical composition of these films switches from SiO_xC_y with CH_3 moieties to SiO_x between 450 and 500°C [10].

Indeed, as a first approximation, we assumed that $E \approx E_f$ and $H \approx H_f$ for thick films. Nevertheless, it is possible that substrate contribution varies with sufficient magnitude, especially for the HMDS films, making the comparison of E and H as functions of T_d inaccurate and preventing the observation of any trend, as h/t ranges from 9.4 to 19.2 % for TEOS thick films and from 14.9 to 20.6 % for HMDS thick films. Therefore, a more reliable analysis may

be possible by using intrinsic E_f and H_f values obtained by modeling, especially for the thin films.

3.2. Initial selection of models

Several models have been proposed for the indentation of films. Two model sets can be identified: the analytical rheological models (with Bec model [19] as the only rheological model) and the empirical models (with every other model listed in Table 3). Analytical rheological models, are built on the physical modeling of the system with elementary rheological elements (i.e. springs, etc.). Empirical models are based on mixing laws: mathematical functions designed empirically to fit the considered data.

Four among the nine reviewed models were originally designed for indenters with disciform contact area: (i.e. flat cylindrical punch, sphere or cone tip): the Bec, the Song-Pharr, the Perriot-Barthel and the Kovalev. These models use "a", the radius of the indenter, as an input variable. In order to adapt these models to the modified Berkovitch tip used in this study, we express "a" as a function of "h", as shown in Equation 3.

$$a = h\sqrt{\frac{24.5}{\pi}} \tag{3}$$

This expression allows to simulate the radius of an indenter with a projected disciform contact area equal to the projected contact area of the modified Berkovitch indenter at a given indentation depth "h".

Table 3 List of the considered models

Model	Output parameters	Model equations	Reference
Bec	E_f	$\frac{1}{E(h)} = \frac{2a}{1+\frac{2t}{\pi a}}\left(\frac{t}{\pi a^2 E_f} + \frac{1}{2aE_s}\right)$ with $a = h\sqrt{\frac{24.5}{\pi}}$	[19,30]
Song-Pharr (Modified Gao)	E_f, ν_f	$\frac{1}{E(a)} = \frac{(1-\nu_s)(1-\nu_f)}{1-(1-I_1(a))\nu_f - I_1(a)\nu_s}\left(\frac{1-I_0(a)}{(1-\nu_s)E_s} + \frac{I_0(a)}{(1-\nu_f)E_f}\right)$ with $I_0(a) = \frac{2}{\pi}Arctan\left(\frac{t}{a}\right) + \frac{1}{2\pi(1-\nu)}\left[(1-2\nu)\frac{t}{a}ln\left(\frac{1+\left(\frac{t}{a}\right)^2}{\left(\frac{t}{a}\right)^2}\right) - \frac{\frac{t}{a}}{1+\left(\frac{t}{a}\right)^2}\right]$, $I_1(a) = \frac{2}{\pi}Arctan\left(\frac{t}{a}\right) + \frac{t}{\pi a}ln\left(\frac{1+\left(\frac{t}{a}\right)^2}{\left(\frac{t}{a}\right)^2}\right)$ and $a = h\sqrt{\frac{24.5}{\pi}}$	[24,31]
Saha-Nix (Modified King)	E_f, ν_f, α	$\frac{1}{E(h)} = \frac{1-\nu_i^2}{E_i} + \frac{1-\nu_f^2}{E_f}\left(1-exp\left(-\frac{\alpha(t-h)}{\sqrt{A_p(h)}}\right)\right) + \frac{1-\nu_s^2}{E_s}exp\left(-\frac{\alpha(t-h)}{\sqrt{A_p(h)}}\right)$ with $A_p(h) = 24.5\,h^2$ for a modified Berkovitch indenter	[20,32]
Martyniuk	E_f, A, C H_f, B, D	$E(h) = E_s\left(\frac{E_f}{E_s}\right)^{L(h)}$ with $L(h) = \frac{1}{1+A\left(\frac{h}{t}\right)^C}$ $H(h) = H_s\left(\frac{H_f}{H_s}\right)^{M(h)}$ with $M(h) = \frac{1}{1+B\left(\frac{h}{t}\right)^D}$	[23]
Korsunsky	H_f, k	$H(h) = H_s + \frac{H_f - H_s}{1+k\left(\frac{h}{t}\right)^2}$	[21,33]
Modified Korsunsky	H_f, β_0, X	$H(h) = H_s + \frac{H_f - H_s}{1+\left(\frac{h}{\beta_0 t}\right)^X}$	[34]

Puchi-Cabrera	H_f, k, m	$H(h) = H_s + (H_f - H_s)e^{-k\left(\frac{h}{t}\right)^m}$	[18]
Perriot-Barthel	E_f, x_0, n	$E(a) = E_s + \frac{E_f - E_s}{1+\left(x_0\frac{t}{a}\right)^n}$ with $a = h\sqrt{\frac{24.5}{\pi}}$	[35]
Kovalev	E_f, λ, τ	$E(a) = E_f + \frac{E_s - E_f}{1+exp\left(-\lambda\frac{E_s - E_f}{E_f}\frac{\frac{a}{t}-\tau}{\tau}\right)}$ with $a = h\sqrt{\frac{24.5}{\pi}}$	[36]

E(h) or E(a): the measured Young modulus (GPa); H(h) or H(a), the measured hardness (GPa)

Input constants: t: film thickness (nm); E_s: intrinsic measured Si(100) substrate Young modulus (172 GPa); H_s: intrinsic measured Si(100) substrate hardness (15.3 GPa); ν_s: Poisson ratio of the Si(100) silicon (0.25 [19,20])

Input variables: a: radius of the indenter (flat cylindrical punch for Bec and Song-Pharr, sphere tip for Kovalev) (nm); h: the indentation depth of the indenter (nm); $A_p(h)$: projected area of the indenter (nm^2)

Output parameters: E_f: intrinsic Young modulus of the film (GPa); H_f: intrinsic hardness of the film (GPa); ν_f: Poisson ratio of the film; α, A, C, B, D, k, β_0, X, m, x'_0, n, λ and τ: fitting parameters

1

TEOS-550°C-713 nm has been selected as the reference sample for the identification of the most suitable models, as it was probed by static nanoindentation at the lowest relative indentation depth (h/t = 9.4 ± 0.1 %, *cf.* Table 2), within the boundaries of Bückle 10 % rule. With this low h/t value, the substrate contribution on E and H is as low as possible. As a consequence, models are selected only by meeting the following criteria: E_f and H_f must be found close to E and H (reliability criterion), respectively, and χ^2_m must be as low as possible (fitting criterion). Every model from Table 3 has been used for TEOS-550-713 nm and the calculated values of E_f, H_f and χ^2_m are displayed in Table 4.

Most of the models met both reliability and fitting criteria and were selected. Bec [19,30] and Song-Pharr [24,37] models present values of χ^2_m higher than the other models. This can be explained as these model use few (or no) output parameters and possess a lower degree of latitude to fit the experimental E(h) vs. h/t and H(h) vs. h/t curves. Thus, these models are not discarded. Finally, only two models were discarded: Kovalev model [36], because it gives an abnormal value of E_f despite an excellent fit and Saha-Nix model [20,32] as it is unusable for h/t > 1 (due to the exponential terms it contains), a situation that is likely to be encountered in thin films. The seven selected models are listed in Table 5.

Table 5 Summary of the models selected using TEOS-550°C-713 nm reference sample

Models for E_f calculation	**Models for H_f calculation**
Martyniuk [23]	
Perriot-Barthel [35]	Korsunsky [21,33]
Bec [19,30]	Modified Korsunsky [34]
Song-Pharr [24,31]	Puchi-Cabrera [18]

3.3. Models validation with thick TEOS samples

The selected models from Table 5 have been tested with the rest of the thick TEOS samples. The resulting E_f and H_f are compared with static indentation values of E and H in Figure 2a and Figure 2b.

As shown by Figure 2a, static indentation E is systematically found superior to E_f values, due to the higher value of E_s. It can be observed that the difference between E and E_f is minimal at 550°C (*i.e.*, for the sample with the lowest value of h/t) which confirms that TEOS-550°C-713 nm was an accurate choice for reference sample. Every model can be considered reliable as they give similar values of E_f.

Figure 2b systematically reveals that $H_f \approx 1.3H$, probably due to a more limited substrate contribution to the hardness measured by static indentation (with $h/t < 20\%$). Finding $H_f > H$ is surprising as substrate contribution was expected to increase the measured hardness (as $H_s = 15.3$ GPa). The lower values found for H than H_f may originate from several sources: models misestimating the substrate contribution on H, mainly sinus measurement inaccuracy for H or possible contribution of a thin soft surface alteration layer that models would neglect. As models systematically give $H_f > H$, the overestimation of substrate contribution seems unlikely. The source of the higher H_f values remains an open question but models can be considered reliable: they consistently give values of E_f and H_f which are close to E and H values, in good agreement with literature values, while at the same time E_f and H_f present a similar evolution with T_d to E and H.

3.4. Models selection for thin films

When tested for thin films, most of the seven models shown in Table 5 fail to find consistent values of E_f or H_f, leading to extremely low or null values (not shown). Only three models (the Bec [19], Song-Pharr [24,31] and Korsunsky [21,33] models) provide consistent values of E_f or H_f (*i.e.* close to the one found for the corresponding thick films and in good agreement with literature for similar silica glass [25,26,28]) as shown in Figure 3a and b for TEOS samples, Figure 4a and b for HMDS samples.

Since every model meets the curve fitting criterion (whether or not they failed to find consistent values of E_f or H_f), the cause of the failure cannot be a poor fitting of the experimental data. An explanation may be the higher level of extrapolation required for thin films: as data obtained for $h < 50$ nm are systematically discarded, the minimal h/t probed for thin films is of about 0.6 (for thick films, it was between 0.09 and 0.2). Only the models with the lowest number of fitting parameters could find consistent values of E_f (Bec and Song-Pharr models) and H_f (Korsunsky model), proving a robustness superior to models with a higher degree of latitude, which is in good agreement with the literature [18]. As an indication of reliability and robustness, these three models have been shown in recent articles [38–40] to characterize efficiently various systems, including coated systems with films of thicknesses similar to the TEOS and HMDS films of the present work.

More interestingly, E_f values calculated for thin and thick films deposited at identical T_d are found consistent and in good correlation with the values of E obtained for the thicker films.

As previously noted, calculated values of E_f are found systematically slightly lower than E for thick (with $E_f \leq E \leq 1.5E_f$) and lower than E for thin films (with $1.4E_f \leq E \leq 2.1E_f$) due to the more or less negligible substrate contribution on system elastic strain. H_f and H values are in close agreement for thick (with $H \approx 0.8H_f$) and thin films (with $H \approx 1.1H_f$) due to the more limited substrate contribution (which may explain why $H \leq H_f$ only for thin films).

This demonstrates the efficient removal of substrate contribution by the selected models. Similar calculated H_f values are found for both thin and thick films deposited at the same of T_d, with the exception of TEOS-400°C-525 nm. Both E_f and H_f values (for thin and thick films) increase with T_d, as expected, considering the previously reported evolution (composition and cross-linking) of the films [12].

A similar comparison between E and E_f and H and H_f is carried out for HMDS thick and thin films and displayed in Figure 4a (for E and E_f) and Figure 4b (for H and H_f), respectively.

As previously observed for TEOS samples, calculated E_f and H_f values for HMDS samples are found close to the static E and H measured for thick films. Due to the smaller substrate contribution on hardness, H_f and H are systematically found close for both thin and thick films (with $H \approx 0.8H_f$ for thick films and $0.7H_f \leq H \leq 1.2H_f$ for thin films).

Whereas measured E shows no clear behavior as a function of T_d, both calculated E_f and H_f increase with T_d, similarly to TEOS samples and in a good agreement with the evolution of the chemical composition of HMDS films.

Finally, the E, E_f, H and H_f values found for HMDS-500°C-500nm sample must be pointed out, as they are consistently and inexplicably lower compared to the rest of the values found.

In summary, from the initial nine tested models, only the Bec, Song-Pharr and Korsunsky models allowed a successful assessment of E_f and H_f for the silica-based coatings of interest within this work. Using calculated E_f and H_f instead of E and H allowed a more accurate correlation between the mechanical properties of TEOS and HMDS samples and the evolution of the chemical composition and structural organization, in better agreement with the literature. It also leads to an expanded range of films thicknesses that can be accurately evaluated through nanoindentation, thus allowing reduced chemical vapor deposition time that was conventionally required for the assessment of film mechanical properties.

4. Conclusion

By associating dynamic indentation experiments with analytical or empirical models, more accurate values of Young modulus and hardness could be calculated for SiO_x and SiO_xC_y to

SiO_x samples obtained from TEOS and HMDS+TEOS, respectively. These calculated values are likely to be closer to the real intrinsic properties of the thin films. Among the nine initially considered models, three could systematically determine E_f and H_f for silicon oxide and silicon oxycarbide films with t ranging from 60 to 700 nm. These are the Bec and Song-Pharr models for the determination of E_f and the Korsunsky model for H_f calculation.

The comparison between measured E and calculated E_f highlighted that Young modulus is more likely to be affected by substrate contribution, as generally expected, even for thick films. For the thinner films (with typical t below 120 nm), the consideration of calculated E_f instead of E is essential, given that extremely high and unrealistic values of E were found for the thinnest films (with values up to 98 ± 3 GPa for TEOS-550°C-95 nm and 95 ± 2 GPa for HMDS-550°C-103 nm). H and H_f exhibited smaller differences as a sign of the more limited substrate influence on hardness.

Using E_f and H_f instead of E and H makes the correlation with the previously characterized chemical composition and the structural organization of TEOS and HMDS samples easier: such a correlation is much more complicated to observe when considering static indentation alone, as the larger influence of the substrate has a levelling effect on the obtained data [10,12]. The consistence of the values found for films of very different thicknesses and obtained from various precursors with expected literature-based values proves the reliability of the method.

In conclusion, dynamic indentation associated to models is a promising tool for the precise study of thin films and superficial events, as it leads to an expanded range of films thicknesses that can be accurately evaluated through nanoindentation technique. Developing new physics-based analytical models, like the rheological model proposed by Bec et al., to simulate the elastoplastic behavior of the film/substrate system with improved accuracy would be of interest to expand the array of available tools. On the other hand, pushing forward the use of models

by characterizing thinner coatings or thin superficial regions of bulk materials, such as the alteration layer on bulk materials or multi-layered materials [22,39,41], still remains an interesting challenge for a better understanding of deposition growth and evolution mechanisms of coated and/or altered systems.

Acknowledgements

The present work was funded by Agence Nationale de la Recherche (ANR) under the contract HEALTHYGLASS ANR-17-CE08-0056.

References

[1] G. Reiter, M. Hamieh, P. Damman, S. Sclavons, S. Gabriele, T. Vilmin, E. Raphaël, Residual stresses in thin polymer films cause rupture and dominate early stages of dewetting, Nat. Mater. 4 (2005) 754. https://doi.org/10.1038/nmat1484.

[2] J. Robertson, R.M. Wallace, High-K materials and metal gates for CMOS applications, Mater. Sci. Eng. R Reports. 88 (2015) 1. https://doi.org/10.1016/j.mser.2014.11.001.

[3] S. Ponton, F. Dhainaut, H. Vergnes, D. Samelor, D. Sadowski, V. Rouessac, H. Lecoq, T. Sauvage, B. Caussat, C. Vahlas, Investigation of the densification mechanisms and corrosion resistance of amorphous silica films, J. Non. Cryst. Solids. 515 (2019) 34. https://doi.org/10.1016/j.jnoncrysol.2019.04.005.

[4] M. Arango-Ospina, F. Xie, I. Gonzalo-Juan, R. Riedel, E. Ionescu, A.R. Boccaccini, Review: Silicon oxycarbide based materials for biomedical applications, Appl. Mater. Today. 18 (2020) 100482. https://doi.org/10.1016/j.apmt.2019.100482.

[5] Y. Shi, L. He, F. Guang, L. Li, Z. Xin, R. Liu, A review: Preparation, performance, and applications of silicon oxynitride film, Micromachines. 10 (2019) 552. https://doi.org/10.3390/mi10080552.

[6] P. Chang, C. Huang, J. Shie, On Liquid-Phase Deposition of Silicon Dioxide by Boric Acid Addition, J. Electrochem. Soc. 144 (1997) 1144. https://doi.org/10.1149/1.1837547.

[7] S.K. Ray, C.K. Maiti, S.K. Lahiri, N.B. Chakrabarti, TEOS-based PECVD of silicon dioxide for VLSI applications, Adv. Mater. Opt. Electron. 6 (1996) 73. https://doi.org/10.1002/(SICI)1099-0712(199603)6:2<73::AID-AMO215>3.0.CO;2-R.

[8] R.-D. Fu, C.K. Chang, M.-Y. Chuang, T.-H. Chen, S.-K. Lu, D.-S. Liu, High

Performance Multilayered Organosilicon / Silicon Oxynitride Water Barrier Structure Consecutively Deposited by Plasma-Enhanced Chemical Vapor Deposition at a Low-Temperature, Coatings. 10 (2020) 11. https://doi.org/https://doi.org/10.3390/coatings10010011.

[9] D. Rats, L. Martinu, J. Von Stebut, Mechanical properties of plasma-deposited SiO_xN_y coatings on polymer substrates using low load carrying capacity techniques, Surf. Coatings Technol. 123 (2000) 36. https://doi.org/10.1016/S0257-8972(99)00381-3.

[10] K.C. Topka, B. Diallo, D. Samelor, R. Laloo, D. Sadowski, C. Genevois, T. Sauvage, F. Senocq, H. Vergnes, V. Turq, N. Pellerin, B. Caussat, C. Vahlas, Tunable SiO_2 to SiO_xC_yH films by ozone assisted chemical vapor deposition from tetraethylorthosilicate and hexamethyldisilazane mixtures, Surf. Coatings Technol. 407 (2021) 126762. https://doi.org/10.1016/j.surfcoat.2020.126762.

[11] Y. Lin, Y. Xiang, T.Y. Tsui, J.J. Vlassak, PECVD low-permittivity organosilicate glass coatings: Adhesion, fracture and mechanical properties, Acta Mater. 56 (2008) 4932. https://doi.org/10.1016/j.actamat.2008.06.007.

[12] B. Diallo, K.C. Topka, M. Puyo, C. Lebesgue, C. Genevois, R. Laloo, D. Samelor, H. Lecoq, M. Allix, H. Vergnes, F. Senocq, P. Florian, V. Sarou-Kanian, T. Sauvage, M.-J. Menu, B. Caussat, V. Turq, C. Vahlas, N. Pellerin, Network hydration, ordering and composition interplay of chemical vapor deposited amorphous silica films from tetraethyl orthosilicate, J. Mater. Res. Technol. 13 (2021) 534. https://doi.org/10.1016/j.jmrt.2021.04.067.

[13] W.C. Oliver, G.M. Pharr, An improved technique for determining hardness and elastic modulus using load and displacement sensing indentation experiments, J. Mater. Res. 7 (1992) 1564. https://doi.org/https://doi.org/10.1557/JMR.1992.1564.

[14] H. Bückle, Progress in micro-indentation hardness testing, Metall. Rev. 4 (1959) 49. https://doi.org/https://doi.org/10.1179/095066059790421746.

[15] E. Broitman, Indentation Hardness Measurements at Macro-, Micro-, and Nanoscale: A Critical Overview, Tribol. Lett. 65 (2017) 23. https://doi.org/10.1007/s11249-016-0805-5.

[16] J. Chen, S.J. Bull, On the factors affecting the critical indenter penetration for measurement of coating hardness, Vacuum. 83 (2009) 911. https://doi.org/10.1016/j.vacuum.2008.11.007.

[17] J. Chen, S.J. Bull, On the relationship between plastic zone radius and maximum depth during nanoindentation, Surf. Coatings Technol. 201 (2006) 4289. https://doi.org/10.1016/j.surfcoat.2006.08.099.

[18] A. Iost, G. Guillemot, Y. Rudermann, M. Bigerelle, A comparison of models for predicting the true hardness of thin films, Thin Solid Films. 524 (2012) 229. https://doi.org/10.1016/j.tsf.2012.10.017.

[19] S. Bec, A. Tonck, J.L. Loubet, A simple guide to determine elastic properties of films on substrate from nanoindentation experiments, Philos. Mag. 86 (2006) 5347. https://doi.org/10.1080/14786430600660856.

[20] R. Saha, W.D. Nix, Effects of the substrate on the determination of thin film mechanical properties by nanoindentation, Acta Mater. 50 (2002) 23. https://doi.org/10.4028/0-87849-999-7.766.

[21] J.R. Tuck, A.M. Korsunsky, R.I. Davidson, S.J. Bull, D.M. Elliott, Modelling of the hardness of electroplated nickel coatings on copper substrates, Surf. Coatings Technol. 127 (2000) 1. https://doi.org/10.1016/S0257-8972(00)00537-5.

[22] M. Kalisz, M. Grobelny, M. Świniarski, M. Mazur, D. Wojcieszak, M. Zdrojek, J. Judek, J. Domaradzki, D. Kaczmarek, Comparison of structural, mechanical and corrosion properties of thin TiO_2/graphene hybrid systems formed on Ti-Al-V alloys in biomedical applications, Surf. Coatings Technol. 290 (2016) 124. https://doi.org/10.1016/j.surfcoat.2015.08.011.

[23] M. Martyniuk, J. Antoszewski, B.A. Walmsley, C.A. Musca, J.M. Dell, Y.-G. Jung, B.R. Lawn, H. Huang, L. Faraone, Determination of mechanical properties of silicon nitride thin films using nanoindentation, Spaceborne Sensors II. 5798 (2005) 216. https://doi.org/10.1117/12.604245.

[24] A. Rar, H. Song, G.M. Pharr, Assessment of new relation for the elastic compliance of a film-substrate system, Mater. Res. Soc. Symp. - Proc. 695 (2002) 431. https://doi.org/10.1557/proc-695-l10.10.1.

[25] B. Jiang, H. He, Y. Zhang, J. Yu, Effects of water immersion and humid weathering on the near-surface mechanical properties of phosphate laser glass, J. Am. Ceram. Soc. 102 (2019) 2462. https://doi.org/10.1111/jace.16083.

[26] H. Mei, Y. Yang, A.C.T. van Duin, S.B. Sinnott, J.C. Mauro, L. Liu, Z. Fu, Effects of water on the mechanical properties of silica glass using molecular dynamics, Acta Mater. 178 (2019) 36. https://doi.org/10.1016/j.actamat.2019.07.049.

[27] H. Lu, H. Cui, I. Bhat, S. Murarka, W. Lanford, W.-J. Hsia, W. Li, Characterization of methyl-doped silicon oxide film deposited using Flowfill^{TM} chemical vapor deposition technology, J. Vac. Sci. Technol. B Microelectron. Nanom. Struct. 20 (2002) 828. https://doi.org/10.1116/1.1470510.

[28] S. Ito, M. Tomozawa, Dynamic Fatigue of Sodium-Silicate Glasses With High Water Content., J. Phys. (Paris), Colloq. 43 (1982) 611.

https://doi.org/10.1051/jphyscol:19829122.

[29] J. Ballarre, D.A. López, A.L. Cavalieri, Nano-indentation of hybrid silica coatings on surgical grade stainless steel, Thin Solid Films. 516 (2008) 1082. https://doi.org/10.1016/j.tsf.2007.07.186.

[30] S. Bec, A. Tonck, J.M. Georges, E. Georges, J.L. Loubet, Improvements in the indentation method with a surface force apparatus, Philos. Mag. A Phys. Condens. Matter, Struct. Defects Mech. Prop. 74 (1996) 1061. https://doi.org/10.1080/01418619608239707.

[31] H. Gao, C.-H. Chiu, J. Lee, Elastic contact versus indentation modeling of multi-layered materials, Int. J. Solids Struct. 29 (1992) 2471. https://doi.org/10.1016/0020-7683(92)90004-D.

[32] R.B. King, Elastic analysis of some punch problems for a layered medium, Int. J. Solids Struct. 23 (1987) 1657. https://doi.org/https://doi.org/10.1016/0020-7683(87)90116-8.

[33] A.M. Korsunsky, M.R. McGurk, S.J. Bull, T.F. Page, On the hardness of coated systems, Surf. Coatings Technol. 99 (1998) 171. https://doi.org/10.1016/S0257-8972(97)00522-7.

[34] A.M. Korsunsky, A. Constantinescu, Work of indentation approach to the analysis of hardness and modulus of thin coatings, Mater. Sci. Eng. A. 423 (2006) 28. https://doi.org/10.1016/j.msea.2005.09.126.

[35] A. Perriot, E. Barthel, Elastic contact to a coated half-space: Effective elastic modulus and real penetration, J. Mater. Res. 19 (2004) 600. https://doi.org/10.1557/jmr.2004.19.2.600.

[36] B. Cappella, D. Silbernagl, Nanomechanical properties of polymer thin films measured by force-distance curves, Thin Solid Films. 516 (2008) 1952. https://doi.org/10.1016/j.tsf.2007.09.042.

[37] G. Huajian, C. Cheng-Hsin, L. Jin, Elastic contact versus indentation modeling of multi-layered materials, Int. J. Solids Struct. 29 (1992) 2471. https://doi.org/10.1016/0020-7683(92)90004-D.

[38] N. Bhaskar, V. Sulyaeva, E. Gatapova, V. Kaichev, D. Rogilo, M. Khomyakov, M. Kosinova, B. Basu, $SiC_xN_yO_z$ Coatings Enhance Endothelialization and Bactericidal activity and Reduce Blood Cell Activation, ACS Biomater. Sci. Eng. 6 (2020) 5571. https://doi.org/10.1021/acsbiomaterials.0c00472.

[39] D. Mercier, V. Mandrillon, G. Parry, M. Verdier, R. Estevez, Y. Bréchet, T. Maindron, Investigation of the fracture of very thin amorphous alumina film during spherical nanoindentation, Thin Solid Films. 638 (2017) 34. https://doi.org/10.1016/j.tsf.2017.07.040.

[40] C.A. Botero, E. Jiménez-Piqué, C. Baudín, N. Salán, L. Llanes, Nanoindentation of Al2O3/Al2TiO5 composites: Small-scale mechanical properties of Al_2TiO_5 as reinforcement phase, J. Eur. Ceram. Soc. 32 (2012) 3723.

[41] D. Mercier, V. Mandrillon, M. Verdier, Y. Brechet, Young's modulus measurement of a thin film from experimental nanoindentation performed on multilayer systems, Mater. Tech. 99 (2011) 169. https://doi.org/10.1051/mattech/2011029.

List of Figures

Table 1 Deposition temperatures T_d and thicknesses t for the investigated samples

Set	Sub-set	Sample	T_d (°C)	t (nm)
TEOS samples	Thin films	TEOS-400°C-98nm	400	98
		TEOS-450°C-102nm	450	102
		TEOS-500°C-128nm	500	128
		TEOS-550°C-95nm	550	95
	Thick films	TEOS-400°C-525nm	400	542
		TEOS-450°C-402nm	450	402
		TEOS-500°C-498nm	500	498
		TEOS-550°C-713nm	550	713
HMDS samples	Thin films	HMDS-400°C-92nm	400	92
		HMDS-450°C-63nm	450	63
		HMDS-500°C-114nm	500	114
		HMDS-550°C-103nm	550	103
	Thick films	HMDS-360°C-703nm	360	703
		HMDS-400°C-525nm	400	525
		HMDS-500°C-500nm	500	500

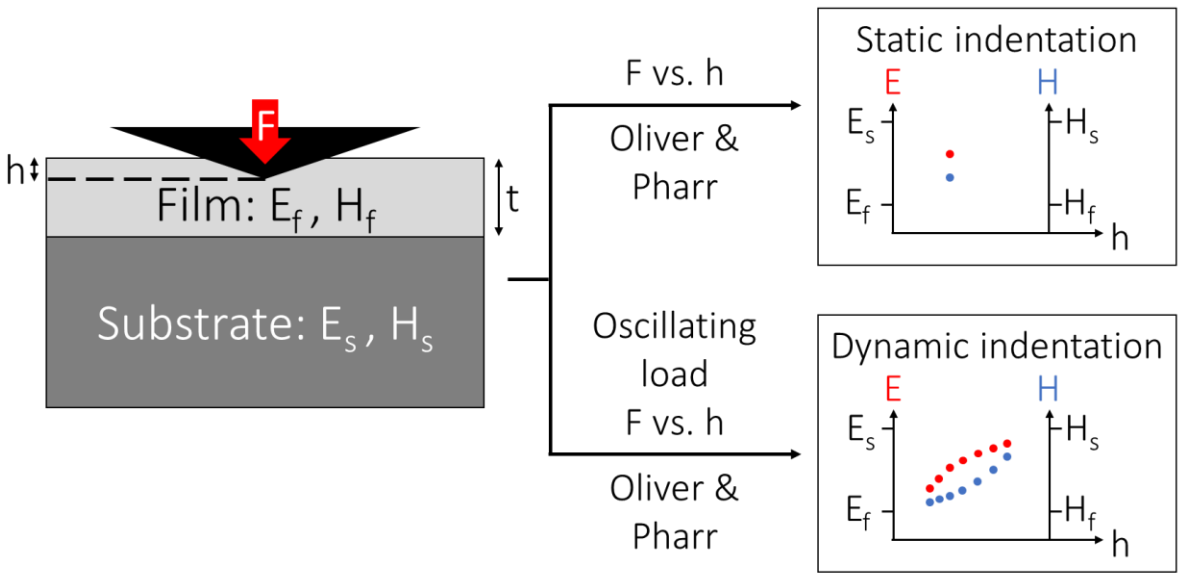

Figure 1 Illustration of the difference between the results of the static and the dynamic indentation (with $E_f < E_s$ and $H_f < H_s$)

Table 2 Values of E and H measured by static nanoindentation for the investigated samples, maximum indentation depth h on film thickness t ratio i.e. relative indentation depth is given for each sample

		Thin films			Thick films		
Set	**T_d (°C)**	**h/t (%)**	**E (GPa)[a]**	**H (GPa)[a]**	**h/t (%)**	**E (GPa)[a]**	**H (GPa)[a]**
TEOS	400	68.9 ± 2.2	89 ± 3	3.9 ± 0.3	14.4 ± 0.3	62 ± 2	7.2 ± 0.4
	450	61.4 ± 2.0	93 ± 4	4.7 ± 0.3	19.2 ± 0.8	51 ± 2	3.6 ± 0.3
	500	45.6 ± 1.1	87 ± 3	5.7 ± 0.3	13.8 ± 0.3	61 ± 2	4.5 ± 0.3
	550	58.1 ± 1.6	98 ± 3	6.1 ± 0.3	9.4 ± 0.1	59 ± 2	5.0 ± 0.1
HMDS	360	-	-	-	14.9 ± 1.6	20 ± 2	1.8 ± 0.2
	400	72.1 ± 3.7	89 ± 6	4.1 ± 0.4	15.4 ± 0.2	48 ± 0(4)	3.3 ± 0.1
	450	102.9 ± 4.7	105 ± 5	4.1 ± 0.4	-	-	-
	500	57.1 ± 1.8	89 ± 2	4.3 ± 0.3	20.6 ± 0.4	29 ± 1	2.2 ± 0.1
	550	57.6 ± 0.7	95 ± 2	5.2 ± 0.2	-	-	-

For reference, E_s = 172 GPa and H_s = 15.3 GPa

[a] Measured with static indentation at 0.5 mN

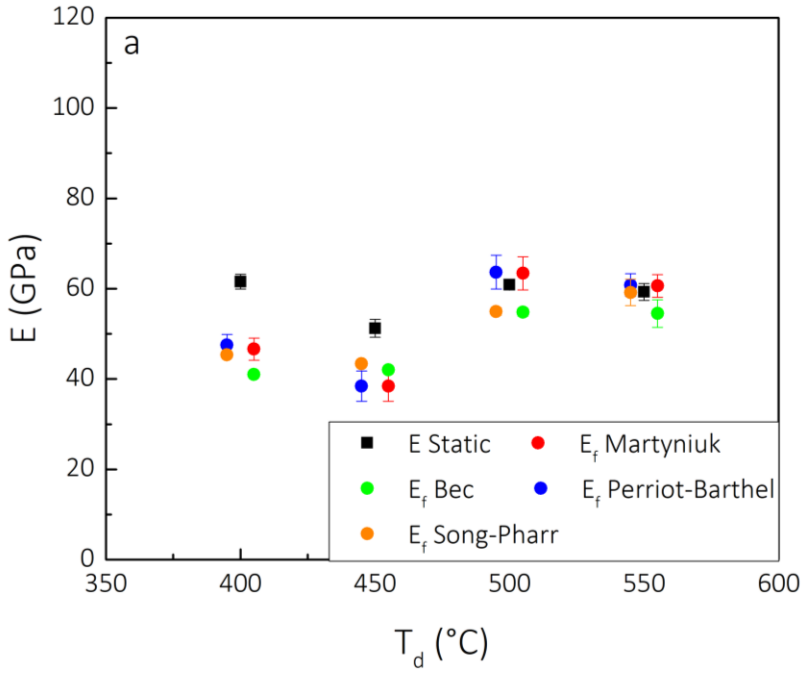

1

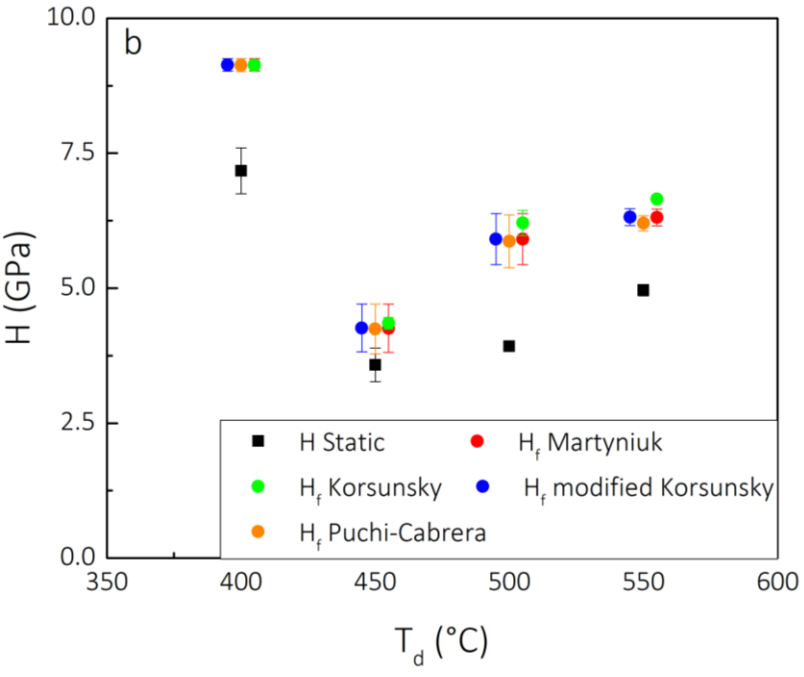

2

3 Figure 2 Variation of (a) experimental E and calculated E_f and (b) experimental H and
4 calculated H_f along T_d for thick TEOS samples (for clarification, data calculated with Perriot-
5 Barthel, Song-Pharr and modified Korsunsky models have been shifted by -5°C and data
6 calculated with Bec, Martyniuk and Korsunsky models have been shifted by +5°C)

7

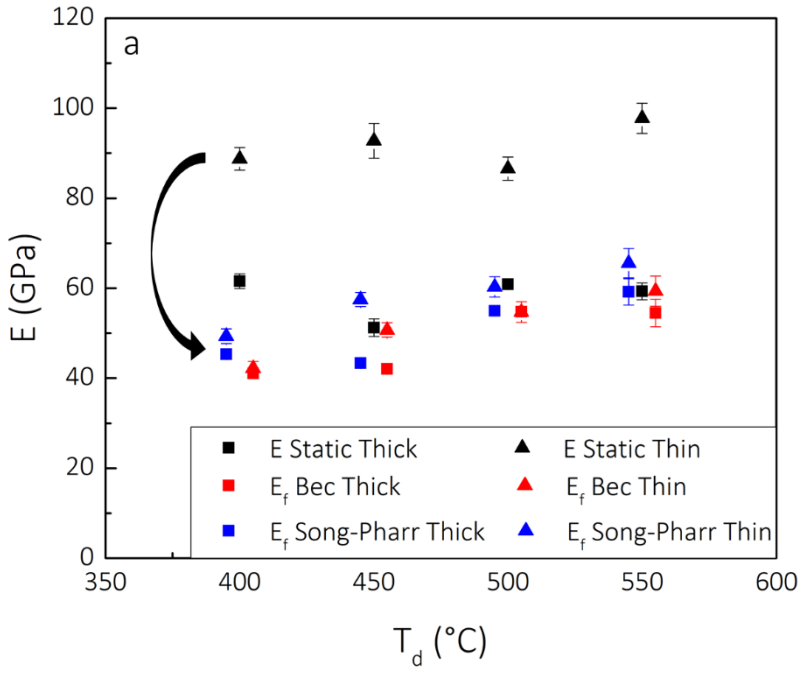

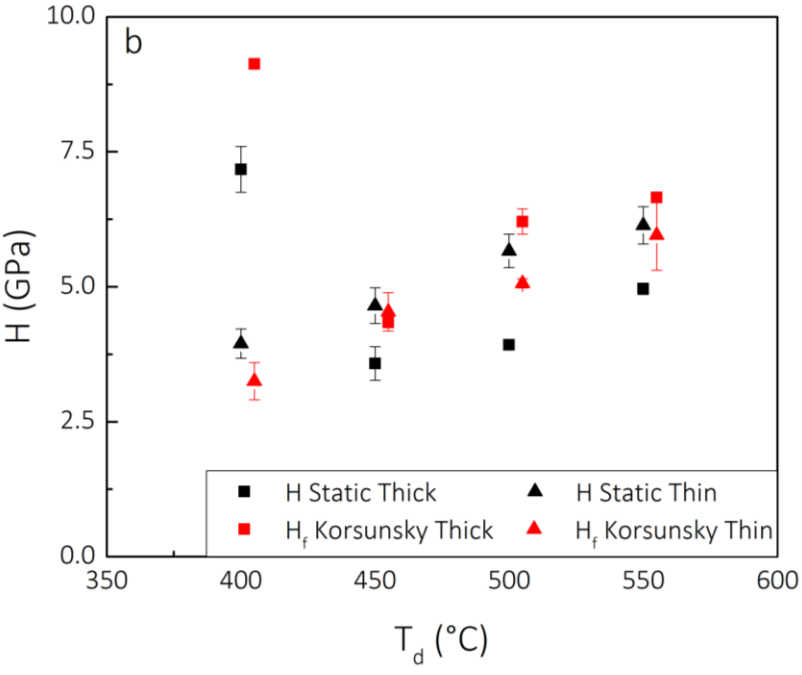

Figure 3 Comparison of (a) experimental E with model calculated E_f and (b) experimental H with model calculated H_f for TEOS samples versus T_d (for clarification, data calculated with Song-Pharr model have been shifted by -5°C and data calculated with Bec and Korsunsky models have been shifted by +5°C)

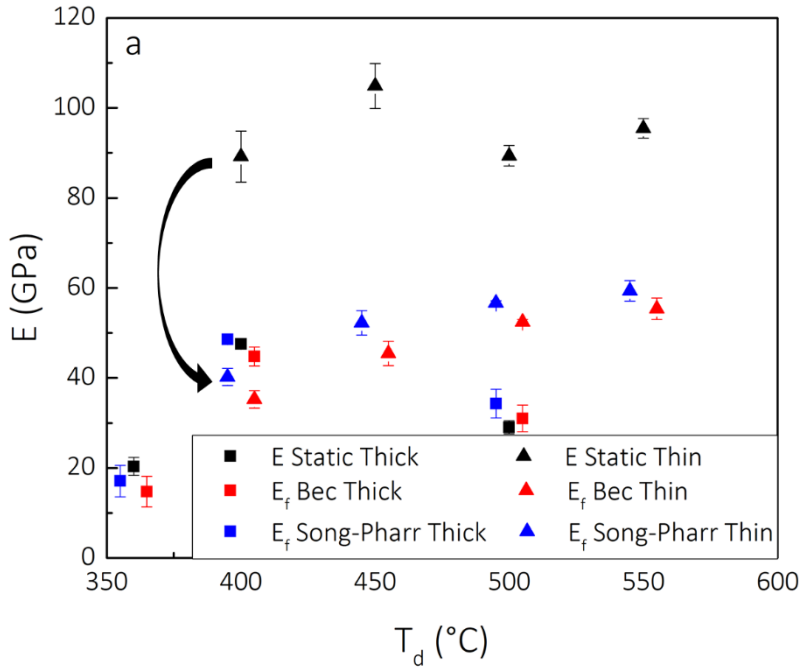

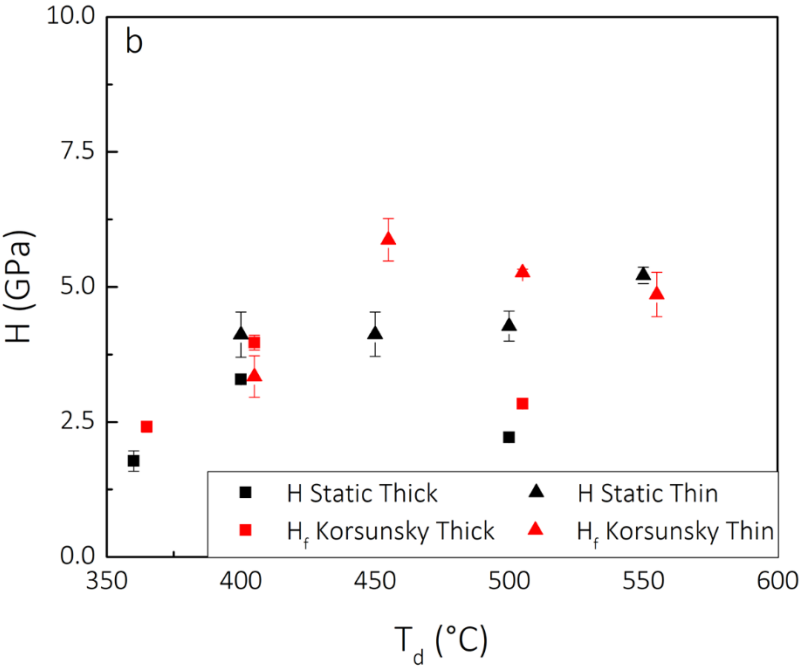

Figure 4 Comparison of (a) experimental E with model calculated E_f and (b) experimental H with model calculated H_f for HMDS samples versus T_d (for clarification, data calculated with Song-Pharr model have been shifted by -5°C and data calculated with Bec and Korsunsky models have been shifted by +5°C)

Table 3 List of the considered models

Model	Output parameters	Model equations	Reference
Bec	E_f	$\frac{1}{E(h)} = \frac{2a}{1+\frac{2t}{\pi a}}\left(\frac{t}{\pi a^2 E_f} + \frac{1}{2aE_s}\right)$ with $a = h\sqrt{\frac{24.5}{\pi}}$	[19]
Song-Pharr (Modified Gao)	E_f, ν_f	$\frac{1}{E(a)} = \frac{(1-\nu_s)(1-\nu_f)}{1-(1-I_1(a))\nu_f - I_1(a)\nu_s}\left(\frac{1-I_0(a)}{(1-\nu_s)E_s} + \frac{I_0(a)}{(1-\nu_f)E_f}\right)$ with $I_0(a) = \frac{2}{\pi}Arctan\left(\frac{t}{a}\right) + \frac{1}{2\pi(1-\nu)}\left[(1-2\nu)\frac{t}{a}ln\left(\frac{1+\left(\frac{t}{a}\right)^2}{\left(\frac{t}{a}\right)^2}\right) - \frac{\frac{t}{a}}{1+\left(\frac{t}{a}\right)^2}\right]$, $I_1(a) = \frac{2}{\pi}Arctan\left(\frac{t}{a}\right) + \frac{t}{\pi a}ln\left(\frac{1+\left(\frac{t}{a}\right)^2}{\left(\frac{t}{a}\right)^2}\right)$ and $a = h\sqrt{\frac{24.5}{\pi}}$	[24,31]
Saha-Nix (Modified King)	E_f, ν_f, α	$\frac{1}{E(h)} = \frac{1-{\nu_i}^2}{E_i} + \frac{1-{\nu_f}^2}{E_f}\left(1-exp\left(-\frac{\alpha(t-h)}{\sqrt{A_p(h)}}\right)\right) + \frac{1-{\nu_s}^2}{E_s}exp\left(-\frac{\alpha(t-h)}{\sqrt{A_p(h)}}\right)$ with $A_p(h) = 24.5\,h^2$ for a modified Berkovitch indenter	[20,32]
Martyniuk	E_f, A, C H_f, B, D	$E(h) = E_s\left(\frac{E_f}{E_s}\right)^{L(h)}$ with $L(h) = \frac{1}{1+A\left(\frac{h}{t}\right)^C}$ $H(h) = H_s\left(\frac{H_f}{H_s}\right)^{M(h)}$ with $M(h) = \frac{1}{1+B\left(\frac{h}{t}\right)^D}$	[23]
Korsunsky	H_f, k	$H(h) = H_s + \frac{H_f - H_s}{1+k\left(\frac{h}{t}\right)^2}$	[21,33]
Modified Korsunsky	H_f, β_0, X	$H(h) = H_s + \frac{H_f - H_s}{1+\left(\frac{h}{\beta_0 t}\right)^X}$	[34]

Puchi-Cabrera	H_f, k, m	$H(h) = H_s + (H_f - H_s)e^{-k\left(\frac{h}{t}\right)^m}$	[18]
Perriot-Barthel	E_f, x_0, n	$E(a) = E_s + \frac{E_f - E_s}{1+\left(x_0\frac{t}{a}\right)^n}$ with $a = h\sqrt{\frac{24.5}{\pi}}$	[35]
Kovalev	E_f, λ, τ	$E(a) = E_f + \frac{E_s - E_f}{1+exp\left(-\lambda\frac{E_s - E_f}{E_f}\frac{\frac{a}{t}-\tau}{\tau}\right)}$ with $a = h\sqrt{\frac{24.5}{\pi}}$	[36]

E(h) or E(a): the measured Young modulus (GPa); H(h) or H(a), the measured hardness (GPa)

Input constants: t: film thickness (nm); E_s: intrinsic measured Si(100) substrate Young modulus (172 GPa); H_s: intrinsic measured Si(100) substrate hardness (15.3 GPa); ν_s: Poisson ratio of the Si(100) silicon (0.25 [19,20])

Input variables: a: radius of the indenter (flat cylindrical punch for Bec and Song-Pharr, sphere tip for Kovalev) (nm); h: the indentation depth of the indenter (nm); $A_p(h)$: projected area of the indenter (nm^2)

Output parameters: E_f: intrinsic Young modulus of the film (GPa); H_f: intrinsic hardness of the film (GPa); ν_f: Poisson ratio of the film; α, A, C, B, D, k, β_0, X, m, x'_0, n, λ and τ: fitting parameters

Table 4 Summary of the calculated values of E_f and, H_f , and χ^2_m found with every model for TEOS-550°C-713 nm thick reference sample

Model	**Output parameters**[a]	**E_f (GPa)** **χ^2_m (MPa)**	**H_f (GPa)** **χ^2_m (MPa)**
Static indentation		59 ± 2[b]	5.0 ± 0.1[b]
Bec	E_f	55 ± 3 *220 ± 140*	
Song-Pharr	E_f, ν_f	59 ± 3 *260 ± 150*	
Saha-Nix	E_f, ν_f, α	71 ± 5 *130 ± 80*	
Martyniuk	E_f, A, C H_f, B, D	61 ± 3 *28 ± 5*	6.3 ± 0.2 *1.7 ± 0.3*
Korsunsky	H_f, k		6.7 ± 0.0(4) *2.2 ± 0.3*
Modified Korsunsky	H_f, β_0, X		6.3 ± 0.2 *1.7 ± 0.3*
Puchi-Cabrera	Hf, k, m		6.2 ± 0.1 *1.6 ± 0.2*
Perriot-Barthel	E_f, x_0, n	61 ± 3 *28 ± 5*	
Kovalev	E_f, λ, τ	0.4 ± 0.1 *30 ± 9*	

[a] E_s, H_s and ν_s are input constants: E_s = 172 GPa, H_s = 15.3 GPa and ν_s = 0.25 [19,20]
[b] Experimental value, measured with h/t = 9.4 ± 0.1 %

1 Table 5 Summary of the selected models for both E_f and H_f calculation of the tested films

Models for E_f calculation	**Models for H_f calculation**
Martyniuk [23]	
Perriot-Barthel [35]	Korsunsky [21,33]
Bec [19,30]	Modified Korsunsky [34]
Song-Pharr [24,31]	Puchi-Cabrera [18]

2

Figures and table captions

Figure 1: Illustration of the difference between the results of the static and the dynamic indentation (with $E_f < E_s$ and $H_f < H_s$)

Figure 2: Variation of (a) experimental E and calculated E_f and (b) experimental H and calculated H_f along T_d for thick TEOS samples (for clarification, data calculated with Perriot-Barthel, Song-Pharr and modified Korsunsky models have been shifted by -5°C and data calculated with Bec, Martyniuk and Korsunsky models have been shifted by +5°C)

Figure 3: Comparison of (a) experimental E with model calculated E_f and (b) experimental H with model calculated H_f for TEOS samples versus T_d (for clarification, data calculated with Song-Pharr model have been shifted by -5°C and data calculated with Bec and Korsunsky models have been shifted by +5°C)

Figure 4: Comparison of (a) experimental E with model calculated E_f and (b) experimental H with model calculated H_f for HMDS samples versus T_d (for clarification, data calculated with Song-Pharr model have been shifted by -5°C and data calculated with Bec and Korsunsky models have been shifted by +5°C)

Table 1: Deposition temperatures T_d and thicknesses t for the investigated samples

Table 2: Values of E and H measured by static nanoindentation for the investigated samples, maximum indentation depth h on film thickness t ratio i.e. relative indentation depth is given for each sample

Table 3 List of the considered models

Table 4: Summary of the calculated values of E_f and, H_f , and χ^2_m found with every model for TEOS-550°C-713 nm thick reference sample

Table 5: Summary of the selected models for both E_f and H_f calculation of the tested films